The organisation and turnover of synaptic proteins within molecular supercomplexes

Katie Morris[1,2], Edita Bulovaite[3], Takeshi Kaizuka[3], Candace Adams[1,2], Noboru Komiyama[3,4,5], Seth G. N. Grant[3,4,*], Mathew H. Horrocks[1,2*].

[1]EaStCHEM School of Chemistry, University of Edinburgh, Edinburgh, EH9 3FJ, United Kingdom.

[2]IRR Chemistry Hub, Institute for Regeneration and Repair, University of Edinburgh, Edinburgh, EH16 4UU, United Kingdom.

[3]Genes to Cognition Program, Centre for Clinical Brain Sciences, University of Edinburgh, Edinburgh EH16 4SB, United Kingdom.

[4]Simons Initiative for the Developing Brain (SIDB), Centre for Discovery Brain Sciences, University of Edinburgh, Edinburgh. EH8 9XD. United Kingdom.

[5]The Patrick Wild Centre for Research into Autism, Fragile X Syndrome & Intellectual Disabilities, Centre for Discovery Brain Sciences, University of Edinburgh, Edinburgh EH8 9XD, United Kingdom.

[*]To whom correspondence may be addressed. Email: seth.grant@ed.ac.uk, or mathew.horrocks@ed.ac.uk

Abstract

Post Synaptic Density 95 (PSD95) is an important scaffolding protein found in the postsynaptic terminal of vertebrate excitatory synapses. PSD95 is required to structurally organize over 80 proteins, including glutamate receptors, signaling, adhesion and other molecules, into ~1.5 MDa supercomplexes within the post-synaptic density. Despite its importance, little is known about the dynamics or heterogeneity of PSD95 in such supercomplexes. We have used single-molecule and super-resolution microscopy to probe the molecular organization of individual

PSD95-containing supercomplexes isolated from mouse brain, revealing the number of PSD95 copies in each supercomplex, and the distances between the individual proteins. We have also examined the dynamic nature of these supercomplexes, discovering that PSD95 is replaced over several days. Importantly, we found that old copies of PSD95 are replaced with new protein within the supercomplexes, independent of whole-supercomplex turnover. This finding suggests the existence of a mechanism that allows for the maintenance of the overall structure of the post-synaptic density, despite the rapid turnover of individual proteins.

Introduction

There are trillions of synapses within the human brain, each one containing a complex proteome that, when disrupted by mutations, can lead to a range of brain diseases. To function, synaptic proteins must undergo higher-order assembly into complexes, supercomplexes and clusters[1,2]. Defining the organization of these is a challenge due to the cellular and molecular complexity of the brain. Of particular interest is the scaffolding protein post-synaptic density 95 (PSD95), an abundant postsynaptic protein found in glutamatergic synapses which plays an important role in synaptic plasticity and memory[3]. PSD95 interacts with over 80 protein partners in supercomplexes, including neurotransmitters, ion channels and adhesion proteins[4,5]. We previously reported that PSD95 resides almost exclusively within ~1.5 MDa supercomplexes, and using a genetic and biochemical strategy, we demonstrated that, on average, two PSD95 protein molecules are present in each supercomplex[2].

A multitude of super-resolution (SR) microscopy approaches have been applied to study the nano-architecture of PSD95 and other proteins in synaptic clusters[6–10]. Here, we extend this work and use single-molecule and SR microscopy to observe endogenous PSD95 fused to either eGFP, mEoS2 or HaloTag (PSD95-GFP, PSD95-mEos, PSD95-HaloTag) in individual supercomplexes present in brain homogenate. Through the direct visualization of individual supercomplexes, we identified that while PSD95 is present at a range of stoichiometries, the majority of supercomplexes contain two copies of PSD95.

The turnover of protein in the brain is important for the control of adaptive processes such as plasticity, synaptic transmission, and learning[11–14]. Recently, we quantified the lifetime of endogenous PSD95 across the mouse brain to develop a Lifetime Synaptome Atlas[15], demonstrating that excitatory synapses have a wide range of PSD95 lifetimes, extending from hours to several months. After classification of the synapses[16], we discovered that the lifespan of each subtype is not influenced by its location in the brain. This implies that subtypes with different lifespans serve as the fundamental elements of the entire brain structure. To determine whether this finding extends to the single-molecule level, we probed the turnover of individual PSD95 proteins within supercomplexes across different regions of the brain, and found that old protein can be replaced with new within the each individual supercomplex. This lends credence to Francis Crick's hypothesis that the chemical modification of single units within dimers of synaptic proteins may enable the long-term storage of memories within molecular structures that are turned over in a matter of days[17].

Results

The arrangement of PSD95 within individual supercomplexes

Single-molecule and SR approaches enable the heterogeneity in populations of proteins to be distinguished, and therefore provide an invaluable tool for studying synaptic molecular supercomplexes isolated from brain homogenate. To achieve this aim, the forebrains from culled heterozygous PSD95-mEoS mice were dissected and homogenized following protocols detailed in Fernandez et al.[5] (see **Methods**) (**Figure 1a**). The supercomplexes were subsequently diluted and immobilized on a glass coverslip and imaged, for the first time, using photoactivated localization microscopy (PALM)[18]. Each PSD95-mEoS molecule within the supercomplexes was localized with a mean precision of 21.8 ± 6.5 nm (mean ± S.D., n = 132,929 localizations across 3 biological repeats). Fourier ring correlation[19] was carried out revealing that the acquired images had a mean resolution of 30 ± 4 nm (mean ± S.D., n = 3 biological repeats). This enabled the spatial relationship between individual PSD95 molecules

to be deduced. Examples of super-resolved supercomplexes are shown in **Figure 1bi**. The number of PSD95 molecules per supercomplex was quantified using custom-written code (**Methods**), and the distribution of stoichiometries is shown in **Figure 1bii**. Over 130,000 PSD95-mEoS proteins were localized in 82,501 supercomplexes across three biological repeats. 76 ± 2 % of the supercomplexes contained only one PSD95-mEoS protein, 12 ± 1 % contained two PSD95-mEoS2 proteins, and the rest (12 ± 2 %) of the clusters contained more than two PSD95-mEoS2 proteins. Given that only half of the PSD95 proteins are fused to mEoS2 in heterozygous mice, and that not all mEoS2 will fold correctly, this suggests that supercomplexes tend to contain more than one PSD95 protein, with the majority containing only two. This is the first time that individual PSD95 supercomplexes from the brain have been visualized, and supports our previous finding that each ~1.5 MDa supercomplex contains, on average, two PSD95 proteins. Class averaging of 9,743 supercomplexes containing two PSD-mEoS proteins showed two clear peaks separated by 37.8 nm (**Figure 1biii**), however, there is a wide distribution of distances (**Figure 1biv**). Previous electron microscopy studies have also detailed the organization of PSD95 in the synapse[20], demonstrating that PSD95 exists as 20-30 nm long filaments within the PSD. As a single PSD95 protein has a length on the order of ~12 nm from the predicted AlphaFold structure[21], it seems reasonable to postulate that the PSD95 filaments identified by electron microscopy are formed from dimers of PSD95, with the measured dimer length of 37.8 nm aligning with the previously published values of 20-30 nm, allowing for linkage error of the fluorophores[20].

To further verify the PSD95 stoichiometry in supercomplexes, photobleaching analysis was carried out on homogenate containing PSD95-GFP supercomplexes (**Figure 1ci**). The mice used for this verification were also heterozygous for PSD95-GFP. Although this technique is diffraction-limited, the number of fluorescent proteins present in a diffraction-limited spot can be quantified by the stepwise photobleaching of each individual fluorophore[22,23]. The number of photobleaching steps per diffraction-limited spot was determined for a population of >47,000 supercomplexes (**Figure 1cii**, with examples of one step and two step photobleaching traces

presented in **Figure 1ciii**). We validated our approach using purified eGFP, demonstrating that the vast majority of eGFP was monomeric (**Figure S1**). The distribution of photobleaching steps resembles that of the number of PSD95-mEoS proteins per supercomplex from the PALM analysis. For the photobleaching analysis, the mean = 1.5 and the mode = 1. For the PALM analysis, the mean = 1.6 and the mode = 1. We also identified multimers in wild-type PSD95 supercomplexes using a mix of orthogonally labeled PSD95 nanobodies (**Figure S2**).

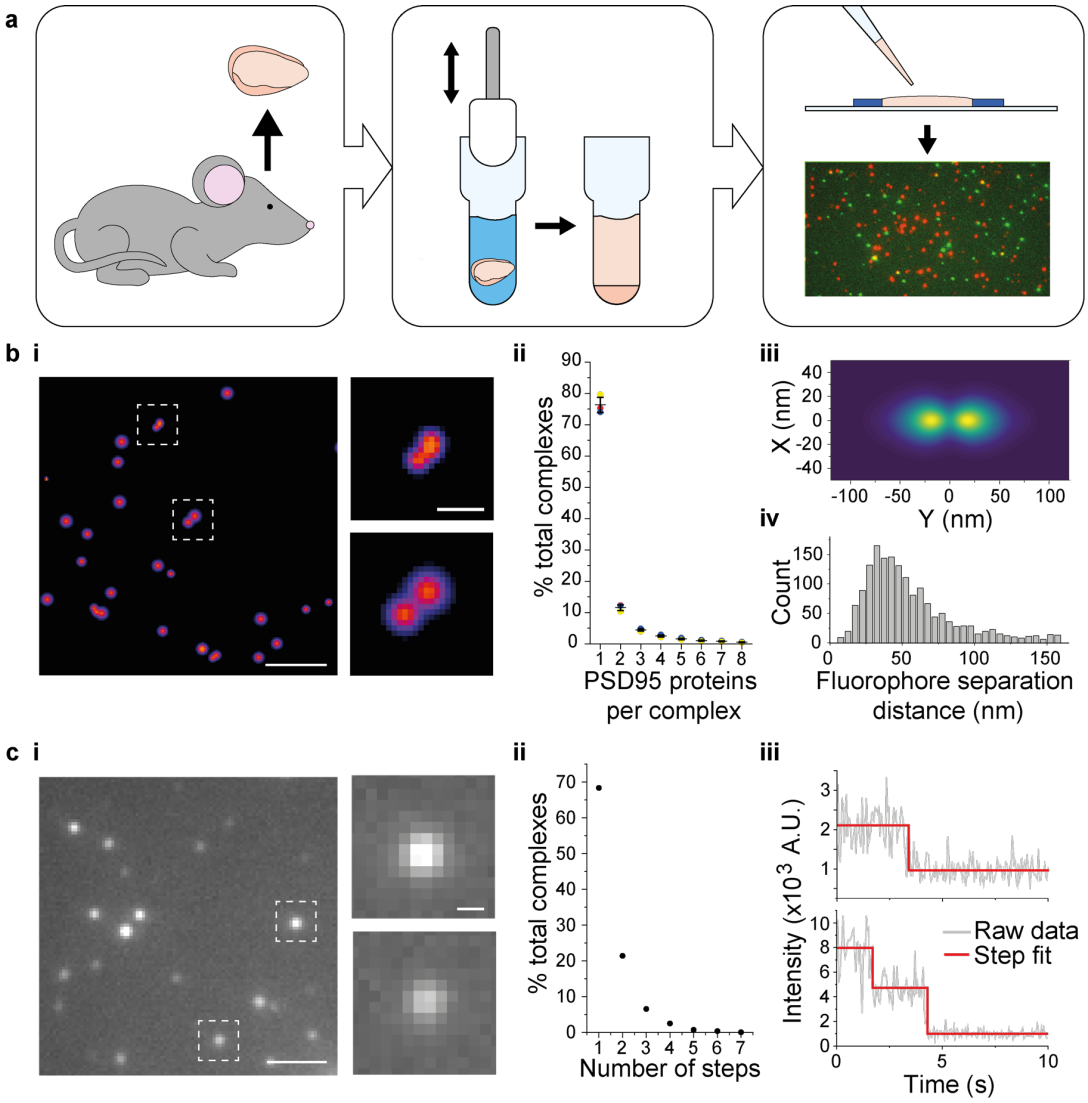

Figure 1. Visualizing PSD95 within individual supercomplexes in mouse brain homogenate. a) *Brain containing either endogenously-tagged PSD95-GFP or PSD95-mEoS was extracted from the genetically-modified mouse, and the forebrain was homogenized to solubilize PSD95-containing supercomplexes. PSD95 supercomplexes were immobilized on*

glass coverslips and imaged using PALM. ***bi)*** *Example PALM images of individual PSD95 supercomplexes. Scale bar = 500 nm, inset scale bar = 50 nm.* ***bii)*** *Subsequent analysis revealed that PSD95 exists at a range of stoichiometries within the supercomplexes (132,929 PSD95-mEoS molecules were detected in 82,501 individual supercomplexes). Plots show mean ± SD, n = 3 biological repeats.* ***biii)*** *Class averaging of the dimer population identified shows a distinct separation between the PSD95 proteins within the supercomplexes (class average of 9,743 supercomplexes).* ***biv****) A histogram of individual distances measured between the two PSD95 molecules in the supercomplexes shows a distribution of the separation distances (peak at 37.8 nm).* ***ci)*** *Individual PSD95-GFP supercomplexes were imaged using TIRF microscopy. Scale bar = 2 µm, inset scale bar = 250 nm. Photobleaching step counting revealed a distribution of PSD95 stoichiometries (presented in* ***cii****) resembling those identified in PSD-mEoS supercomplexes (71,178 PSD95-GFP photobleaching steps were counted across 47,211 supercomplexes). Representative intensity traces with fits shown in* ***ciii.*** *Photobleaching of individual fluorophores result in a step-wise decrease in intensity.*

PSD95 protein turnover in PSD95 supercomplexes

We have previously measured the rate of turnover of PSD95 across the brain, demonstrating that excitatory synapses have a wide range of protein lifetimes extending from a few hours to several months[15]. This allowed us to define short protein lifetime (SPL) and long protein lifetime (LPL) synapses. After successfully identifying two units of PSD95 within the majority of supercomplexes, our next objective was to investigate whether protein exchange takes place within each supercomplex or if the entire supercomplex is replaced.

To achieve this, we took advantage of a homozygous PSD95-HaloTag mouse, and tagged all of the PSD95-HaloTag by injecting a cell- and blood brain barrier-permeable fluorescent ligand, Silicon-Rhodamine-Halo (SiR-Halo) into the tail vein of three-month-old homozygous PSD95-HaloTag mice (**Figure 2a**)[15]. Because SiR-Halo forms a covalent bond with the PSD95-HaloTag, by examining the persistence of labeling after injection by culling the mice

at different time-points, we were able to determine the lifetime of the PSD95 in individual supercomplexes. Brain tissue was obtained at either 6 hours post-injection or 7 days post-injection. The homogenized forebrain tissue from each mouse was then incubated with a second HaloTag ligand, Alexa-Fluor-488-Halo (AF488-Halo). The AF488-Halo ligand labeled the new PSD95-HaloTag protein that was generated post SiR-Halo injection. This allowed us to quantify the levels of PSD95 protein turned over in 7 days. Supercomplexes containing only SiR-Halo represent those in which no PSD95 exchange had occurred, while those with only AF488-Halo are either new supercomplexes, or supercomplexes in which all PSD95 has been replaced. Finally, those with both SiR-Halo and AF488-Halo give rise to a coincident signal, and represents supercomplexes in which only some of the PSD95 has been exchanged (**Figure 2a**).

Figure 2b shows example diffraction-limited images of the labeled PSD95 supercomplexes at the two time points. Homogenate from mice culled 6 hours post SiR-Halo injection is described as day 0. Most of the supercomplexes observed at day 0 contain only SiR-Halo, with few having AF488-Halo, and negligible coincidence. At day 7, fewer SiR-Halo supercomplexes were observed, indicating that some of the protein present at the time of injection was degraded. An increase in the number of AF488-Halo labeled supercomplexes indicates that the degraded protein has been replaced with new, label-free protein that has subsequently been labeled with AF488-Halo in the post-homogenization incubation. An increase in coincidence can be seen in the merge of the two images. These results are shown quantitatively in **Figure 2c.** Approximately 50% of the old protein appears to have been replaced by new protein between day 0 and day 7. Of the 13,710 supercomplexes analyzed at day 0, 96% of the supercomplexes were labeled with only SiR-Halo, indicating that the HaloTag binding sites were saturated by injection. At day 7, 36.8% of the 15,391 supercomplexes analyzed were labeled with only SiR-Halo. 36.9% of the supercomplexes were labeled with only AF488-Halo, indicating whole supercomplexes had been turned over in the 7-day period. Interestingly, 26.3% of the supercomplexes were labeled with both AF488-

Halo and SiR-Halo, indicating that some supercomplexes contain both old and new protein. This suggests that protein turnover is independent of whole-supercomplex turnover.

Next, the number of PSD95 molecules per supercomplex was quantified using photobleaching analysis. For SiR-Halo- (**Figure 2d**) and AF488-Halo-only (**Figure 2e**) labeled supercomplexes, the number of labels per supercomplex, on average, appears to be approximately 2 at both day 0 and day 7. For mixed supercomplexes at day 7, the average number of PSD95 proteins per supercomplex is greater than two. This indicates that mixed supercomplexes may consist of more than one dimer pair, but supports the theory that proteins, rather than whole supercomplexes, are turned over. Number distributions for **Figure 2c-e** are presented in **Figure S3**.

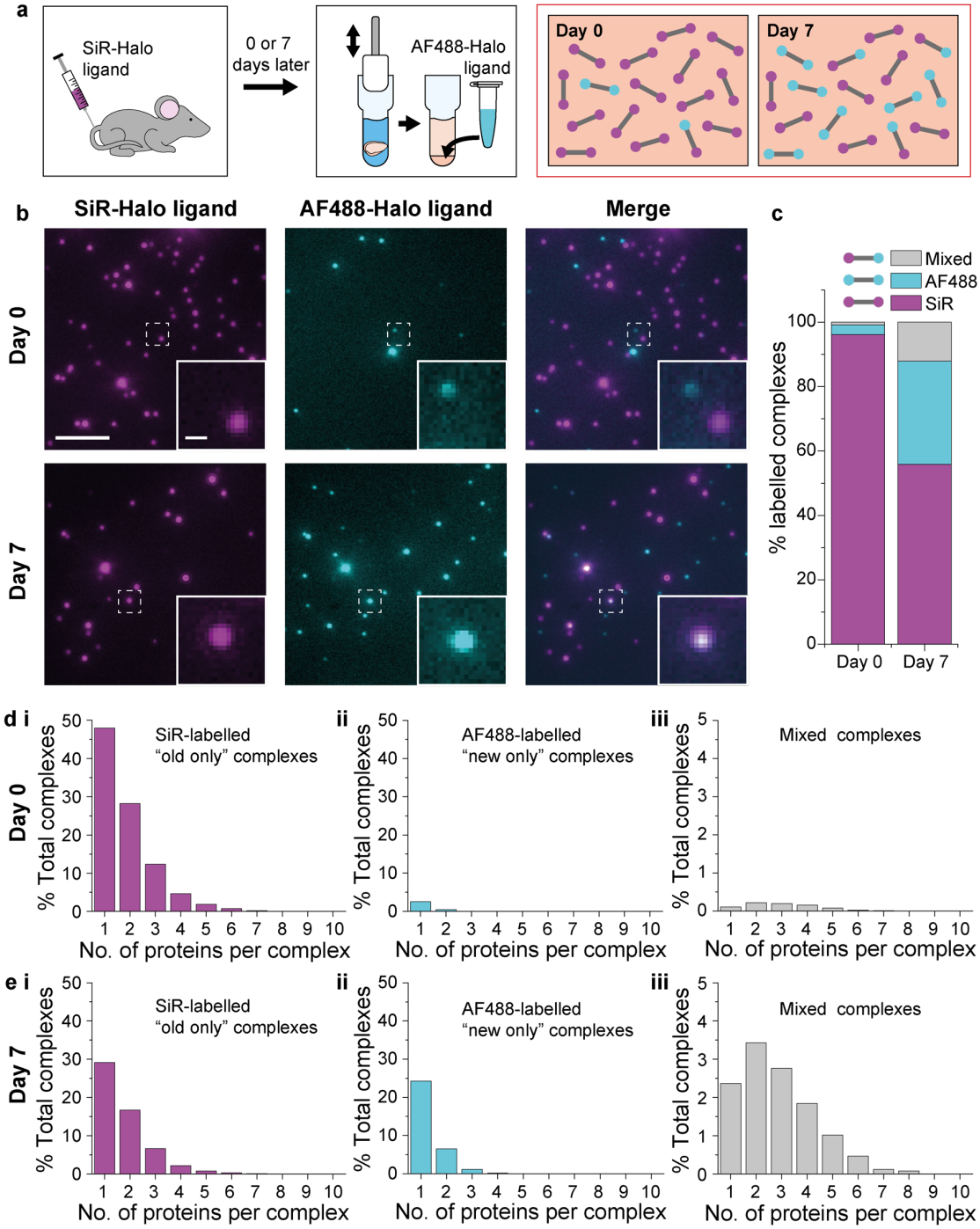

***Figure 2. Characterizing PSD95 turnover within supercomplexes in mouse brain homogenate**. **a)** Homozygous PSD95-HaloTag mice were injected with SiR-Halo ligand. 1 mouse was culled 6 hours post injection and 1 mouse was culled 7 days post injection. The forebrains of the animals were homogenized and post-hoc stained with AF488-Halo ligand to saturate remaining binding sites. At day 0, most of the PSD95 is labeled with only SiR-Halo. After 7 days of protein turnover, 3 populations of supercomplex are possible: those with only*

SiR-Halo, those with only AF488-Halo, and a final population labeled with both fluorophores. ***b)*** *Images of supercomplexes from homogenate at day 0 and day 7, showing increased ratios of AF488-Halo:SiR-Halo at day 7, with increased coincidence.* ***c)*** *Quantified percentages of supercomplexes labeled only with SiR-Halo, AF488-Halo or both. At day 0, 96 % of the supercomplexes were labelled only with SiR, indicating saturation of PSD95-HaloTag binding sites by injection. At day 7, 37 % of supercomplexes were labelled only with SiR, indicating protein turnover has occurred over the 7 days.* ***d,e)*** *The number of fluorophore labels in each supercomplex were counted using photobleaching analysis. The analysis for day 0 is shown in d), and the analysis for day 7 timepoint is shown in e).*

Comparison of synaptic PSD95 to total PSD95

We next sought to probe whether individual protein turnover occurs within synaptic supercomplexes, and not just the ones located elsewhere in the cells. To achieve this, the brains were removed 7 days post SiR-Halo injection, and synaptosomes prepared as described previously[24,25] (see **Methods**). The resulting synaptosomes were incubated in sodium deoxycholate containing buffer for 1 hour to solubilize the synaptic membrane and release the PSD95 containing supercomplexes (**Figure 3a**). After incubation with AF488-Halo, the supercomplexes were imaged using TIRF microscopy. While the level of SiR-Halo-only supercomplexes is similar for both the forebrain and synaptic fractions (56 % and 52%, respectively), the percentage of AF488-Halo-only supercomplexes is lower in the synaptic fraction (21% in the synaptic fraction, 32% in the forebrain), and instead, there is a greater fraction of mixed supercomplexes (27% in the synaptic fraction, and 12% in the forebrain) (**Figure 3b**). This suggests that while the overall rate of PSD95 turnover is similar in the synapses compared to the overall forebrain, there is a greater fraction of supercomplexes that retain at least one old PSD95 protein, underlying their importance in maintaining the overall molecular state of the postsynaptic density. The number of PSD95 molecules per supercomplex from the synaptic fraction is similar to that from the overall brain (**Figure 3c**).

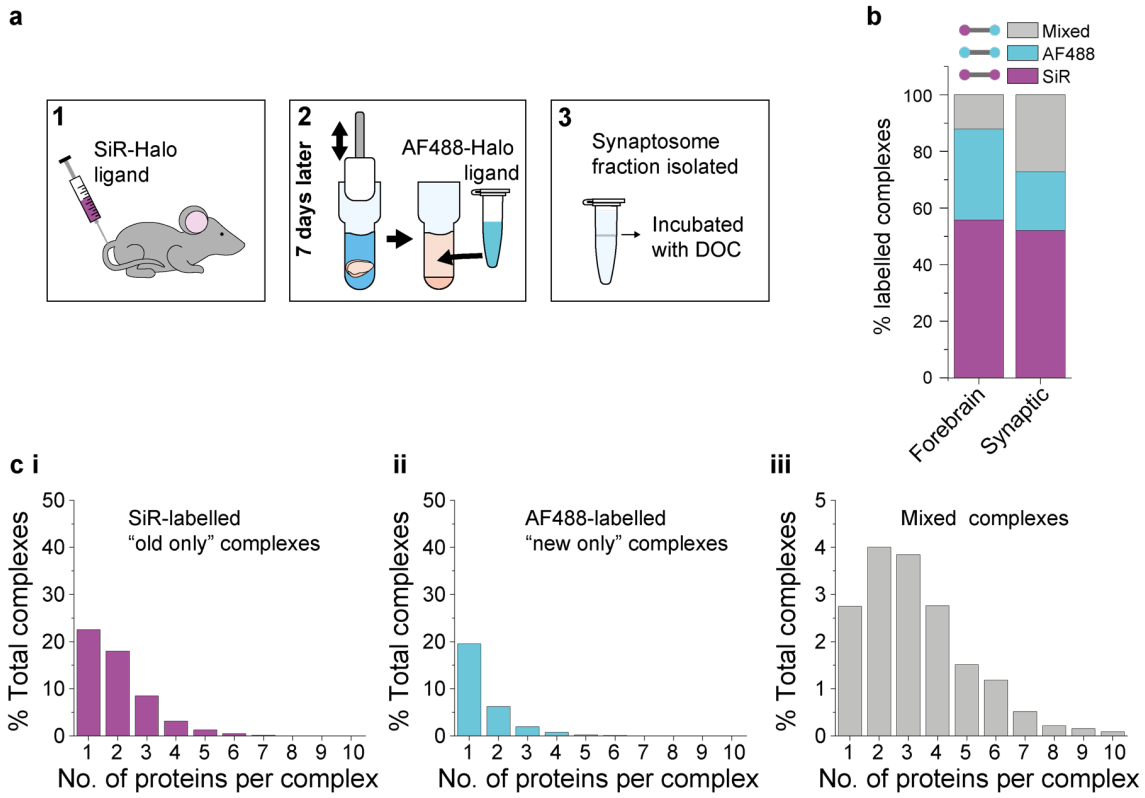

Figure 3. Protein turnover in synaptic and total PSD95 supercomplexes ***a)*** *A cartoon representation of the experimental procedure. SiR-Halo ligand was injected into the tail vein of three 3-month-old PSD95-HaloTag knock-in mice. 7 days later, the forebrain was extracted and synaptosomes isolated. AF488-HaloTag ligand was incorporated during the homogenization process.* ***b)*** *A comparison between the populations of PSD95 supercomplexes in the whole forebrain and PSD95 supercomplexes only found in the synaptic fraction.* ***c)*** *Graphs showing the number of proteins per supercomplex in the synaptic fraction for the SiR-Halo-labeled "old only" supercomplexes* ***(i),*** *AF488-Halo-labeled "new only" supercomplexes* ***(ii)*** *and mixed supercomplexes* ***(iii)****.*

Region-to-region comparison of PSD95 protein turnover

Having observed substantial turnover of PSD95 in the whole forebrain after 7 days, we next investigated whether protein turnover differs between brain areas. Six 3-month-old homozygous PSD95-HaloTag mice were injected with SiR-Halo into the tail vein as previously described. The mice were culled 7 days post-injection. The whole brain of each animal was

extracted and dissected into five broad brain regions: isocortex, hippocampus, olfactory bulb, cerebellum and subcortex (see **Figure 4a**). The brain region homogenates were incubated with AF488-Halo to label new PSD95-Halo proteins and imaged using TIRF microscopy. This allowed us to quantify the turnover of PSD95-Halo on a region-specific basis.

The percentage of supercomplexes containing only old or new protein are shown in **Figure 4bi,** and **Figure 4bii**, respectively. This gives an indication of the rate of protein turnover. Regions with higher percentages of supercomplexes containing only new protein must be turning over protein faster. From **Figure 4bii,** the olfactory bulb has the highest percentage (40 ± 16 %, mean ± SD) of such supercomplexes, and the isocortex has one of the lowest percentages (27 ± 8 %, mean ± SD). Conversely, the isocortex shows the highest percentage (19 ± 3 %, mean ± SD) of mixed supercomplexes, and the olfactory bulb has the lowest percentage (4 ± 3 %, mean ± SD) (**Figure 4biii**). This pattern was also seen in 3-week-old mice (see SI, **Figure S4**). The percentage of supercomplexes containing only old, new or both old and new PSD95 are shown quantitatively as heatmaps in **Figure 4c.** In total, 60,798 supercomplexes were analyzed in the isocortex, 15,842 in the hippocampus, 3,148 in the olfactory bulb, 36,126 in the cerebellum and 28,339 in the subcortical areas.

The correlation between the percentage of PSD95 proteins contained in old, new and mixed supercomplexes in each brain region was compared with the previously published half-life of PSD95 in the same regions (see SI, **Figure S5**)[15]. While there is limited correlation between the percentage of PSD95 proteins contained in old or new supercomplexes and the half-lives of PSD95 puncta in each region, there is a statistically significant correlation between the percentage of PSD95 proteins contained in mixed supercomplexes and the half-lives of PSD95 puncta, with a Pearson's correlation test value of $R = 0.95$ at a significance level of $P = 0.01$.

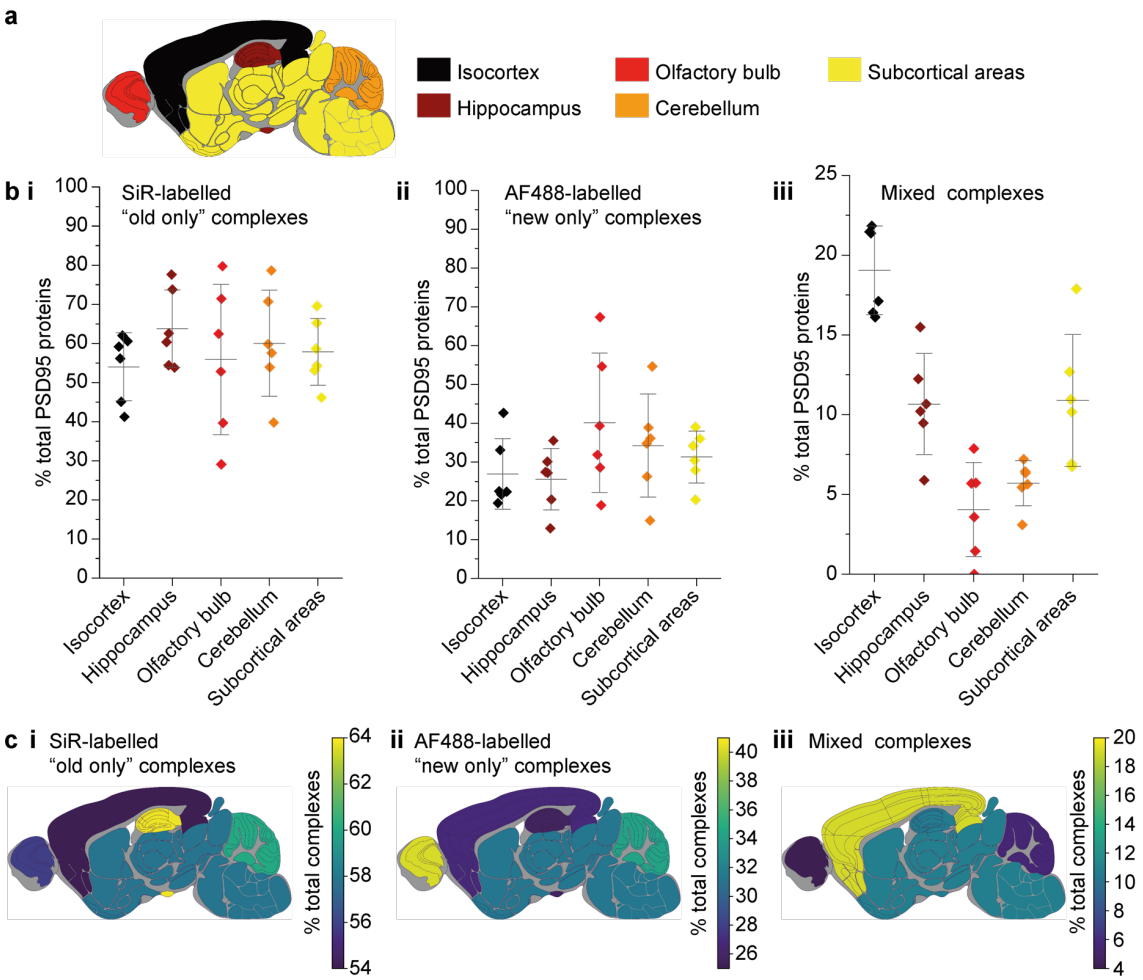

***Figure 4. Differences in PSD95 turnover between mouse brain regions**. **a)** A key showing the five broad brain regions that the mouse brains were dissected into. These regions are the isocortex, hippocampus, olfactory bulb, cerebellum and subcortical areas. **b**) Graphs showing the percentage of total PSD95 imaged contained in SiR-labelled "old only" supercomplexes (**i**), AF488-labelled "new only" supercomplexes (**ii**) and mixed supercomplexes containing both SiR-labelled and AF488-labelled protein (**iii**). Error bars show the standard deviation of 6 biological repeats. **c)** Brain maps showing the percentage of SiR-labelled "old only" (**i**), AF488-labelled "new only" (**ii**) and mixed (**iii**) PSD95 supercomplexes in each region of the brain. For statistical significance, see SI (Table S1).*

Discussion

The application of single-molecule and SR microscopy to study genetically-encoded, fluorescently-tagged PSD95 has enabled us to reveal the structure of individual supercomplexes at the nanometer length scale. While we have previously used biochemical approaches to demonstrate that two copies of PSD95 exist in each supercomplex, this study represents the first direct observation of PSD95 dimers in these megadalton supercomplexes. By using multiple single-molecule and SR microscopy techniques to image the brain homogenate from three mouse models (PSD95-HaloTag, PSD95-GFP, PSD95-mEoS), we have robustly cross-validated our approach for studying the organization of PSD95 in individual supercomplexes. Unlike ensemble averaging techniques, a major advantage of our approach is the ability to observe and quantify hundreds of thousands of PSD95 molecules in tens of thousands of individual supercomplexes, allowing the stoichiometry in each one to be determined, as well as the distances between the PSD95 molecules. Furthermore, by tagging PSD95-HaloTag with specific Halo ligands *in vivo*, followed by culling and imaging at a different time-points, our approach allows the lifetime of PSD95 in individual supercomplexes to be measured. Careful dissection of the brain prior to homogenization and imaging also enables our methods to be deployed for generating maps of structure and lifetime of supercomplexes in different brain regions.

Previous studies have shown that PSD95 shows remarkable structural diversity at the nanometer scale within nanoclusters, and at the micron scale in overall post-synaptic densities[6,10]. Indeed, by quantifying levels of PSD95 and SAP102, we have identified 37 synapse subtypes in the brain. We now show that this synatpic heterogeneity extends to the individual supercomplex level, and demonstrate that while the majority of supercomplexes contain only two PSD95 molecules, there are others that contain more. With the enhanced resolution of PALM, we were also able to measure the distances between individual PSD95 molecules within the supercomplexes and find that rather than being fixed, there is considerable variation in these lengths, with the mean separation distance equaling 37.8 nm.

This could reflect a difference in the molecular make-up of each supercomplex. Indeed, they are composed of dozens of proteins, the identity and arrangement of which are likely to vary significantly.

Having previously shown turnover of PSD95 in the brain, and that different regions have varying PSD95 lifetimes[15], we next sought to determine whether we could detect protein turnover within the supercomplexes. By injecting mice with SiR-Halo to saturate all PSD95-HaloTag proteins, and culling at either day 0 or day 7, we used TIRF microscopy to identify individual supercomplexes that contained either old protein only, new protein only, or a mix of old and new protein. This demonstrates that not only does PSD95 have varying lifetimes at the ensemble level, but that PSD95 turnover in individual supercomplexes also occurs at various rates.

Francis Crick observed that the turnover rate of biomolecules is too fast to account for long-term memories that can last for extended periods[17]. To resolve this paradox, he proposed a model involving multimeric proteins, where subunits can modify each other, for example by phosphorylation. In this model, inactive subunits can exchange into the active multimeric proteins, thereby maintaining the overall structure and modification. The discovery here of individual PSD95 molecules exchanging within supercomplexes directly supports this model, providing insight into the storage of long-term memories. Through the isolation of supercomplexes extracted from synaptosomes, we also demonstrated that synaptic supercomplexes had a greater fraction of mixed old and new PSD95 and a lower fraction of new only PSD95 compared with the brain overall. This suggests that the process of replacing old copies of PSD95 with new copies preferentially occurs within the postsynaptic terminal. Whether this occurs because of stochastic events facilitated by the close packing of supercomplexes within the synapses or by specific mechanisms is unknown.

A regional investigation of supercomplex PSD95 lifetime showed that there was variation across the brain. The highest level of mixed supercomplexes was found in the cortex where the synaptic puncta with the longest PSD95 puncta lifetime (LPL synapses) reside, suggesting that LPL synapses house more of the mixed supercomplexes than SPL synapses. Future studies that address the molecular composition of old, mixed and new supercomplexes may reveal insights into how these supercomplexes control synaptic function and learning and memory.

Methods

Preparation of mouse brain homogenates

Homogenates were prepared from dissected brains or whole mouse forebrains, as described previously[1]. Deoxycholate (DOC) extraction buffer was prepared and stored on ice prior to homogenization and contained 1% sodium deoxycolate, 50 mM tris(hydroxymethyl)aminomethane (tris) pH 9.0, 50 mM sodium fluoride, 20 μM zinc chloride, 1 mM sodium ortho-vanadate, 2 mM 4-(2-aminoethyl)-benzene-sulfonyl fluoride and 1 complete protease inhibitor cocktail tablet (Roche, Germany) per 50 mL.

For whole brain homogenization, each forebrain was added to 5 mL of DOC buffer and homogenized using 20 strokes with a 5 mL capacity Teflon homogenizer. The homogenate was stored on ice for 1 hour, homogenizing again using 20 strokes at 30 minutes. The homogenate was centrifuged at 50,000g for 30 minutes at 4°C. The supernatant was separated from the pellet and contained the PSD95 supercomplexes.

For dissected brain homogenization, each dissected brain region was added to 0.6 mL of DOC buffer. Homogenization and centrifugation was carried out as described above for whole brain specimens, except pellet pestles (Fisher scientific) were used instead of a teflon homogenizer to homogenize the tissue.

Preparation of synaptosome fractions

Adult (5-month-old) PSD95-HaloTag mice were subjected to injection of HaloTag ligand conjugated with SiR as described previously[15]. Seven days after injection, the mice were sacrificed with cervical dislocation and the forebrain was dissected. They were briefly rinsed with ice-cold PBS, frozen with liquid nitrogen, and stored at –80℃ before use. For synaptosome preparation, homogenization of tissue was performed by 12 strokes with Teflon-glass homogenizer in Homogenization buffer (0.32 M sucrose, 1 mM HEPES pH 7.4, and complete EDTA-free Protease Inhibitor Cocktail (Merck)). Brain homogenate was centrifuged at 1,400 g for 10 min at 4℃ to obtain the pellet and the supernatant fraction. The pellet fraction was resuspended in Homogenization buffer with 3 strokes of the homogenizer and centrifuged at 700 g for 10 min at 4℃. The supernatant of the first and second centrifugation was pooled as an S1 fraction and subjected to the subsequent centrifugation at 14,000 g for 10 min at 4℃. The resulting pellet was resuspended with Homogenization buffer (P2 fraction) and centrifuged in a sucrose density gradient (0.85/1.0/1.2 M) for 2 h at 82,500 g. The fraction between 1.0 M and 1.2 M was collected and used as synaptosome.

Dissection of mouse brain regions

Mice were culled by cervical dislocation and decapitated. The brains were removed from the skull and quickly washed with ice-cold PBS. Brains were dissected on ice, on a plastic plate covered with 3MM filter paper soaked in ice-cold PBS. The cerebellum and olfactory bulbs were removed first, then the hippocampus and cortex were isolated from the rest of the brain. Brain samples were snap frozen in liquid nitrogen and stored at -80°C.

For the protein turnover experiments, homozygous PSD95$^{HaloTag/HaloTag}$ knock-in mice were injected with 200 µL 1.5 mM of SiR-Halo ligand diluted in saline and Pluronic F-127 (20% in DMSO). As a control, some injected mice were culled 6 hours post injection to provide a 0-

day timepoint with maximum saturation. The rest of the mice were culled 7 days post injection. Their brains were extracted and prepared as forebrain or region-specific homogenates as described above. Prior to imaging, the turnover homogenates were incubated with 10 μM AF488-Halo ligand in a 1:1 volumetric ratio for 1 hour at 4°C.

TIRF microscopy

All diffraction-limited and PALM experiments were conducted on a home-built TIRF microscope described previously[26]. Briefly, collimated laser light at 405 nm (Cobolt MLD 405–250 Diode Laser System, Cobalt, Sweden), 488 nm (Cobolt Fandango-300 DPSS Laser System, Cobalt, Sweden), 561 nm (Cobolt DPL561-100 DPSS Laser System, Cobalt, Sweden), and 638 nm (Cobolt MLD Series 638-140 Diode Laser System, Cobolt AB, Solna, Sweden) was aligned and directed parallel to the optical axis at the edge of a 1.49 NA TIRF Objective (CFI Apochromat TIRF 60XC Oil), mounted on an inverted Nikon TI2 microscope. The microscope was fitted with a perfect focus system to auto-correct the z-stage drift during imaging. Fluorescence collected by the same objective was separated from the returning TIR beam by a dichroic mirror Di01-R405/488/561/635 (Semrock, Rochester, NY, USA), and was passed through appropriate filters (488 nm: BLP01-488R-25, FF01-525/30-25, 561 nm: LP02-568RS, FF01-587/35, 638 nm: FF01-432/515/595/730-25, LP02-647RU-25, Semrock, Rochester, NY, USA). Fluorescence was then passed through a 2.5× beam expander and recorded on an EMCCD camera (Delta Evolve 512, Photometrics) operating in frame transfer mode (EMGain = 11.5 e-/ADU and 250 ADU/photon). Each pixel was 103 nm in length. Images were recorded with an exposure time of 50 ms. The microscope was automated using the open-source microscopy platform Micromanager. Borosilicate glass coverslips (20 × 20 mm, VWR International) were cleaned using an Ar plasma cleaner (Zepto, Diener) for 30 min to remove any fluorescent residues. Frame-Seal slide chambers (9 × 9 mm^2, Biorad) were affixed to the glass to create a well in which samples (100 μL) were added. All samples in the wells were washed 3x with PBS prior to imaging.

For diffraction-limited photobleaching analysis of GFP, the neat homogenate was diluted 100x in PBS and irradiated and imaged with 488 nm (68 W cm^{-2}, 25 s), ensuring all molecules were photobleached. For diffraction-limited photobleaching analysis of SiR and AF488, whole forebrain homogenate and DOC treated synaptosomes were diluted 100x in PBS. Homogenates from dissected brain regions were diluted 1000-10,000x in PBS. The samples were first irradiated and imaged with 638 nm light (850 W cm^{-2}, 25 s), followed by 488 nm light (110 W cm^{-2}, 25 s), ensuring all molecules were photobleached. For PALM imaging, the samples were diluted 100x in PBS and illuminated with 15 cycles of 405 nm (75 W cm^{-2}, 1 s) and 561 nm (1500 W cm^{-2}, 10 s) irradiation until all molecules were photobleached. In preparation for imaging, samples were incubated on the glass surface for 30 seconds prior to washing 3x with 0.02 µm filtered PBS.

Coincidence analysis

Coincidence analysis was carried out using a custom written MATLAB script. Initially, all spots in the diffraction limited images were detected using the Find Maxima function in ImageJ. The prominences used varied depending upon the fluorophores and the power of the lasers, but generally were ~500-1000. The locations of all spots in both channels were loaded into MATLAB. The distances between the nth spot in the first channel and all spots in the second channel were calculated. Any spots with a separation distance less than the channel offset parameter (2 pixels in this work) were classed as being “coincident”. Finally, the number of spots in the first channel, the number of spots in the second channel, and the number of coincident spots were output by the script.

All scripts used in this analysis are available at: DOI: 10.5281/zenodo.8059239

Photobleaching analysis

Photobleaching data were collected using the TIRF microscope described above, and analyzed using a previously published approach[27,28]. The intensity of the emitted fluorescence from all molecules was tracked over a period of 25 seconds. The intensity traces from each

molecule were extracted by finding spots in the first frame of the image stack using the ImageJ Find Maxima function. The intensity at each spot location was then measured in all frames of the stack using a custom written ImageJ macro. Chung-Kennedy filtering was performed on the resulting intensity traces using a custom written MATLAB script, with a shuttling window size of 12. The Chung-Kennedy filter[29] shuttles two windows along the data set either side each data point. The output of the Chung-Kennedy filter is a weighted average of the mean of the two windows. The weighting shifts the output value towards the mean of the window with the lowest variance such that noise is reduced, but discontinuities in the data do not become blurred during the filtering process.

To detect photobleaching steps in the filtered traces, an approximate differential of the filtered data was calculated. Peaks in the differentiated intensity traces indicated a sharp change in gradient in the intensity trace and thus the position of the photobleaching steps. A peak threshold of 75 was applied to the differentiated intensity traces to extract the location of the steps. The validity of each of the steps was determined by calculating the ratio of individual step height to the local regional variance. This calculation returned a T statistic for each potential step. A T threshold of 0.1 was applied to distinguish true steps from false steps. True steps have large ratios of step height to local regional variance and thus larger T statistics. False steps have smaller ratios of step height to local regional variance and thus smaller T statistics. Once the location of each step was known and the validity confirmed, a step function was generated as a fit to the raw step data.

All scripts used in this analysis are available at: DOI: 10.5281/zenodo.7118670

PALM analysis

The data were preliminarily analyzed using the Peak Fit function of the GDSC SMLM ImageJ plugin to output super-resolved localizations of the blinking fluorophores. A signal strength threshold of 20 was used, along with a precision threshold of 40 nm. Following this, the drift was corrected for using the Drift Calculator function in the GDSC SMLM ImageJ plugin. Once

the localizations were extracted, a custom written MATLAB clustering script was used. The clustering script sorted all localizations by precision from low precision to high precision. To correct for multiple blinks emanating from the same fluorophore, the script consolidated all localizations within the precision of another localization into one object. The distances between all objects were then calculated. Objects separated by less than 160 nm were grouped into clusters. The number of objects in each cluster were counted. Clusters containing one object were defined as “monomeric”, clusters containing two objects were defined as “dimeric” etc. Information pertaining to the clusters (number of objects, x-y position of objects, average precision) was output as a text file.

Class averaging was performed on the class of clusters containing two objects by another custom written MATLAB script. The script aligns all dimeric clusters parallel to the x axis and centers them about the midpoint between the two objects. The objects are plotted as width = precision, and the resulting density at each x-y position is calculated to give the surface plot showing the class average.

All scripts used in this analysis are available at: DOI: 10.5281/zenodo.7993694

Acknowledgements

The single-molecule instruments used in this study were funded by the UK Dementia Research Institute, UCB Biopharmaceuticals, and a kind donation from Dr. Jim Love. T. K. was funded by a Uehara Memorial Foundation Research Fellowship and a Marie Skłodowska-Curie Actions Individual Fellowship. C.A. was funded by the BBSRCEastBIO doctoral training program (BB/M010996/1). S. G. N. G. acknowledges funds from the Simons Foundation Autism Research Initiative (529085), ERC (695568) and a Wellcome Technology Development Grant(202932/Z/16/Z). We would also like to thank Noelia Pelegrina-Hidalgo, Zuzanna Konieczna , and the Biological Chemistry 2 undergraduate students at the University of Edinburgh School of Chemistry for providing purified eGFP.

Author contributions

K.M.: Conceptualization, experimental work, data analysis, and writing. E.B.: Experimental work, data analysis, and writing. T.K.: Experimental work, data analysis, and writing. C.A.: Experimental work, data analysis and writing. N.K.: Experimental work and writing S.G.N.G.: Conceptualization, funding acquisition, supervision, and writing, M.H.H.: Conceptualization, funding acquisition, supervision, and writing.

Competing interests

The authors declare that the research was conducted in the absence of any commercial or financial relationships that could be construed as a potential conflict of interest.

Materials & Correspondence

Correspondence to Seth G. N. Grant or Mathew H. Horrocks.

References

1. Frank, R. A. W. *et al.* NMDA receptors are selectively partitioned into complexes and supercomplexes during synapse maturation. *Nature Communications* **7**, (2016).
2. Frank, R. A. W., Zhu, F., Komiyama, N. H. & Grant, S. G. N. Hierarchical organization and genetically separable subfamilies of PSD95 postsynaptic supercomplexes. *Journal of Neurochemistry* **142**, 504–511 (2017).
3. Migaud, M. *et al.* Enhanced long-term potentiation and impaired learning in mice with mutant postsynaptic density-95 protein. *Nature* **396**, 433–439 (1998).
4. Husi, H., Ward, M. A., Choudhary, J. S., Blackstock, W. P. & Grant, S. G. N. Proteomic analysis of NMDA receptor-adhesion protein signaling complexes. *Nature neuroscience* **3**, 661–669 (2000).
5. Fernández, E. *et al.* Targeted tandem affinity purification of PSD-95 recovers core postsynaptic complexes and schizophrenia susceptibility proteins. *Molecular systems biology* **5**, (2009).

6. Broadhead, M. J. *et al.* PSD95 nanoclusters are postsynaptic building blocks in hippocampus circuits. *Sci Rep* **6**, 24626 (2016).
7. Masch, J.-M. *et al.* Robust nanoscopy of a synaptic protein in living mice by organic-fluorophore labeling. *Proceedings of the National Academy of Sciences* **115**, E8047–E8056 (2018).
8. Han, Y. *et al.* Neuroligin-3 confines AMPA receptors into nanoclusters, thereby controlling synaptic strength at the calyx of Held synapses. *Science Advances* **8**, eabo4173 (2022).
9. Sun, S.-Y. *et al.* Correlative Assembly of Subsynaptic Nanoscale Organizations During Development. *Front Synaptic Neurosci* **14**, 748184 (2022).
10. MacGillavry, H. D., Song, Y., Raghavachari, S. & Blanpied, T. A. Nanoscale scaffolding domains within the postsynaptic density concentrate synaptic AMPA receptors. *Neuron* **78**, 615–622 (2013).
11. Patrick, G. N., Bingol, B., Weld, H. A. & Schuman, E. M. Ubiquitin-Mediated Proteasome Activity Is Required for Agonist-Induced Endocytosis of GluRs. *Current Biology* **13**, 2073–2081 (2003).
12. Kato, A., Rouach, N., Nicoll, R. A. & Bredt, D. S. Activity-dependent NMDA receptor degradation mediated by retrotranslocation and ubiquitination. *Proceedings of the National Academy of Sciences* **102**, 5600–5605 (2005).
13. Ehlers, M. D. Activity level controls postsynaptic composition and signaling via the ubiquitin-proteasome system. *Nat Neurosci* **6**, 231–242 (2003).
14. Colledge, M. *et al.* Ubiquitination Regulates PSD-95 Degradation and AMPA Receptor Surface Expression. *Neuron* **40**, 595–607 (2003).
15. Bulovaite, E. *et al.* A brain atlas of synapse protein lifetime across the mouse lifespan. *Neuron* **110**, 4057-4073.e8 (2022).
16. Zhu, F. *et al.* Architecture of the Mouse Brain Synaptome. *Neuron* **99**, 781-799.e10 (2018).
17. Crick, F. Neurobiology: Memory and molecular turnover. *Nature* **312**, 101–101 (1984).

18. Betzig, E. *et al.* Imaging Intracellular Fluorescent Proteins at Nanometer Resolution. *Science* **313**, 1642–1645 (2006).
19. Nieuwenhuizen, R. P. J. *et al.* Measuring image resolution in optical nanoscopy. *Nat Methods* **10**, 557–562 (2013).
20. Chen, X. *et al.* Organization of the core structure of the postsynaptic density. *Proceedings of the National Academy of Sciences* **105**, 4453–4458 (2008).
21. Jumper, J. *et al.* Highly accurate protein structure prediction with AlphaFold. *Nature* **596**, 583–589 (2021).
22. Dalton, C. E. *et al.* Single-Molecule Fluorescence Detection of a Synthetic Heparan Sulfate Disaccharide. *Chemphyschem* **17**, 3442–3446 (2016).
23. Leake, M. C. *et al.* Stoichiometry and turnover in single, functioning membrane protein complexes. *Nature* **443**, 355–358 (2006).
24. Roy, M. *et al.* Proteomic analysis of postsynaptic proteins in regions of the human neocortex. *Nat Neurosci* **21**, 130–138 (2018).
25. Carlin, R. K., Grab, D. J., Cohen, R. S. & Siekevitz, P. Isolation and characterization of postsynaptic densities from various brain regions: enrichment of different types of postsynaptic densities. *J Cell Biol* **86**, 831–845 (1980).
26. de Moliner, F. *et al.* Small Fluorogenic Amino Acids for Peptide-Guided Background-Free Imaging. *Angewandte Chemie International Edition* **62**, e202216231 (2023).
27. Chappard, A. *et al.* Single-Molecule Two-Color Coincidence Detection of Unlabeled alpha-Synuclein Aggregates. *Angewandte Chemie International Edition* **62**, e202216771 (2023).
28. Choi, M. L. *et al.* Pathological structural conversion of α-synuclein at the mitochondria induces neuronal toxicity. *Nat Neurosci* **25**, 1134–1148 (2022).
29. Chung, S. H. & Kennedy, R. A. Forward-backward non-linear filtering technique for extracting small biological signals from noise. *Journal of Neuroscience Methods* **40**, 71–86 (1991).